Progress In Electromagnetics Research C, Vol. 121, 107–125, 2022

Wideband and Circularly Polarized Designs of Modified E-Shape Microstrip Antennas for GSM and GPS Applications

Venkata A. P. Chavali* **and Amit A. Deshmukh**

Abstract—Variations of modified E-shape microstrip antennas are proposed which realize wideband and circularly polarized responses inside the same impedance bandwidth but in separate frequency regions. The offset pair of slots in E-shape patch tunes the spacing in between TM_{02}, TM_{10}, and TM_{11} mode frequencies, and for the design in 900 MHz frequency band, it yields the total impedance bandwidth of 34.15%, in which circularly polarized bandwidth of 4.75% is present towards the higher frequency region. In comparison with the wideband E-shape or its circularly polarized variation, the proposed configurations yield larger total impedance and same axial ratio bandwidth, but without overlapping bands for the wideband and circularly polarized regions. A compact half E-shape microstrip antenna is proposed, which yields total impedance bandwidth of 38.8%, with a circularly polarized bandwidth of 5.3%, present towards the higher frequency region. Further, the wideband E-shape variations are presented on a thinner substrate by using a bow-tie shape ground plane profile. Against the conventional ground plane design, it offers more than 12% increase in the bandwidth for $0.03\lambda_g$ reduction in the substrate thickness. Thus, as against the reported E-shape variations, the proposed study presents a new design feature of traditional E-shape patch that provides separate regions for the wideband and circularly polarized responses, occupying the same impedance bandwidth.

1. INTRODUCTION

The microstrip antenna (MSA) in the simplest form consists of a radiating patch on one side of the grounded substrate [1]. In earlier days, MSA was regarded as a narrow bandwidth (BW) design [1]. However, over the last three-four decades, many techniques have been evolved to increase the MSA BW. The fundamental concept that lies behind BW increment is the addition of multiple resonant modes. This leads to the designs of gap-coupled and stacked MSAs [1, 2]. While maintaining the low-profile nature of the MSA, the BW is increased by cutting the slot inside the patch [3]. Here, different slot shapes, like U-slot, rectangular slot, and their variations using either coaxial feed or different feed variations on electrically thicker substrate, have been explored [3–16]. In broadband MSAs, radiation pattern over the BW shows polarization purity thereby offering a lower cross-polar levels. In wireless applications where the signal loss due to the interference and multi-path propagation effects is to be minimized, antennas offering higher cross polar level or circular polarized (CP) response are preferred. The CP response in MSA is realized by using the techniques like slot cut in the patch, stub placed on the patch edges, use of the shorting posts, modified shape for the radiation patch, use of parasitic elements, and by embedding fractal slot geometries on the ground plane [17–30]. By embedding resonant a U-slot or a pair of rectangular slots (E-shape) inside the rectangular MSA (RMSA), CP response has been realized [31–33]. These configurations yield axial ratio (AR) BW of 4–5% on a thicker substrate. The dual band CP design of modified E-shape MSA is reported in [34], whereas a compact CP design using a single rectangular slot inside the RMSA is reported in [35]. However, in [31–33, 35], an explanation

Received 21 April 2022, Accepted 16 June 2022, Scheduled 11 July 2022
* Corresponding author: Venkata A. P. Chavali (cpriyag14@gmail.com).
The authors are with the EXTC the Department, SVKM's DJSCE, Mumbai, India.

about the functioning of slot cut antenna in terms of orthogonal resonant modes present and subsequent design methodology is not given, whereas the design reported in [34] requires larger patch size. The dual band CP design using slot cut stacked patches as reported in [36] requires higher antenna volume. The characteristics mode-based analysis for U-slot and E-shape CP MSA designs is reported in [37]. The characteristics mode-based approach does not provide any design guidelines for realizing similar CP antennas in the other frequency band. Furthermore, the impedance BW realized in theseresonant slots cut CP designs is smaller, and it overlaps with the AR BW. Therefore across the impedance BW, polarization of the E-field changes. Similarly in various wideband designs using resonant slots, CP response over a portion of the impedance BW is not achieved.

In this paper, coaxially fed designs of offset E-shape and half E-shape MSAs are presented for the broadband and CP response together. Initially, a detailed parametric study is presented that explains the resonant modes present in the pair of slots cut rectangular MSA (RMSA), which yields wideband and CP response. An offset pair of slots in E-shape MSA tunes the spacing in between TM_{10}, TM_{02}, and TM_{11} resonant modes which achieves the wideband response followed by a CP response. A simulated BW for reflection coefficient (S_{11}) < -10 dB of 302 MHz (32.33%) is achieved, in which towards the higher frequencies of the BW, a CP AR BW of 41 MHz (3.9%) is present. In half E-shape MSA, a rectangular slot tunes the spacing in between the TM_{10}, TM_{01}, and TM_{11} resonant modes which yields wideband response followed by the CP characteristics. In this design, the overall impedance BW of 350 MHz (37.1%) is obtained, which includes the CP AR BW of 48 MHz (4.5%) towards the higher frequency region. Both of these MSAs exhibit broadside radiation pattern with peak gain of more than 8 dBi. The above designs are presented on an electrically thicker substrate ($h \sim 0.07\lambda_g$). To reduce the substrate thickness (probe feed length) for the same patch dimensions,a bow-tie shape ground plane design in both the E-shape MSA variations and a modified beveled feed design for a smaller size half E-shape MSA is presented. In offset E-shape MSA, bow-tie shape ground plane yields impedance BW of 47.13% and AR BW of 4.58%, for $0.03\lambda_g$ reduction in the total substrate thickness. On the other hand, for the feed probe thickness of $0.0216\lambda_g$, beveled fed half E-shape MSA yields an overall impedance BW of 405 MHz (41.3%) that contains CP AR BW of 56 MHz (5.3%), present towards the higher frequency range. By studying the surface current distribution at the modified patch modes, a resonant length formulation followed by the design methodology is presented. This yields similar coaxially fed wideband and CP designs in the desired frequency range. Thus, as against the reported variations, the present study puts forward a new design feature of the E-shape MSA that offers a wideband and CP response, together without their overlap frequency bands. A detailed comparison for the proposed MSAs against the reported work is presented further in the paper. The proposed antennas are initially optimized using IE3D software. An experimental validation is carried out using ZVH-8, FSC 6, and SMB 100 A. A reference wideband Horn antenna is used in the pattern measurement, carried out inside the Antenna lab. Three-antenna method is used to measure the broadside gain.

2. OFFSET E-SHAPE MSA FOR WIDEBAND AND CP RESPONSE

The coaxial fed design of an E-shape MSA is shown in Figures 1(a) and (b). The units of the patch dimensions and frequencies referred throughout the paper are in cm and MHz, respectively. The patch is fabricated on an FR4 substrate ($\varepsilon_r = 4.3$, $h = 0.16$), and it is suspended above the ground plane using an air gap of thickness h_a cm. On the total substrate thickness of 2.16 cm, i.e., $h_a = 2$ cm, equivalent RMSA dimensions are parametrically optimized for TM_{10} mode frequency of 850 MHz. Thus, here RMSA length (L) and width (W) are 13 and 15 cm, respectively. By cutting the pair of rectangular slots on one of the radiating edges of RMSA, an E-shape MSA is realized. As the BW optimization process for the E-shape MSA is well described in the literature, the same is not presented here. For $l_s = 8.5$, $w_s = 0.8$, y_1 & $y = 2.4$, $y_f = 0$, $x_f = 3.6$ cm, E-shape MSA yields impedance BW of 203 MHz (18.6%). The wideband E-shape MSA exhibits broadside radiation pattern over the BW with lower cross polar levels. Across the BW, it offers the AR value of more than 15 dB, to exhibit a linear polarization (LP). In the reported CP designs of E-shape MSA, unequal slot lengths is present, and it offers smaller impedance BW. Also due to the CP response, polarization of the radiated field changes across the BW. To realize a wideband response, modal currents on the patch should be unidirectional, and for the CP response, currents should be bi-directional [31]. In wideband E-shape MSA, equal slot lengths are

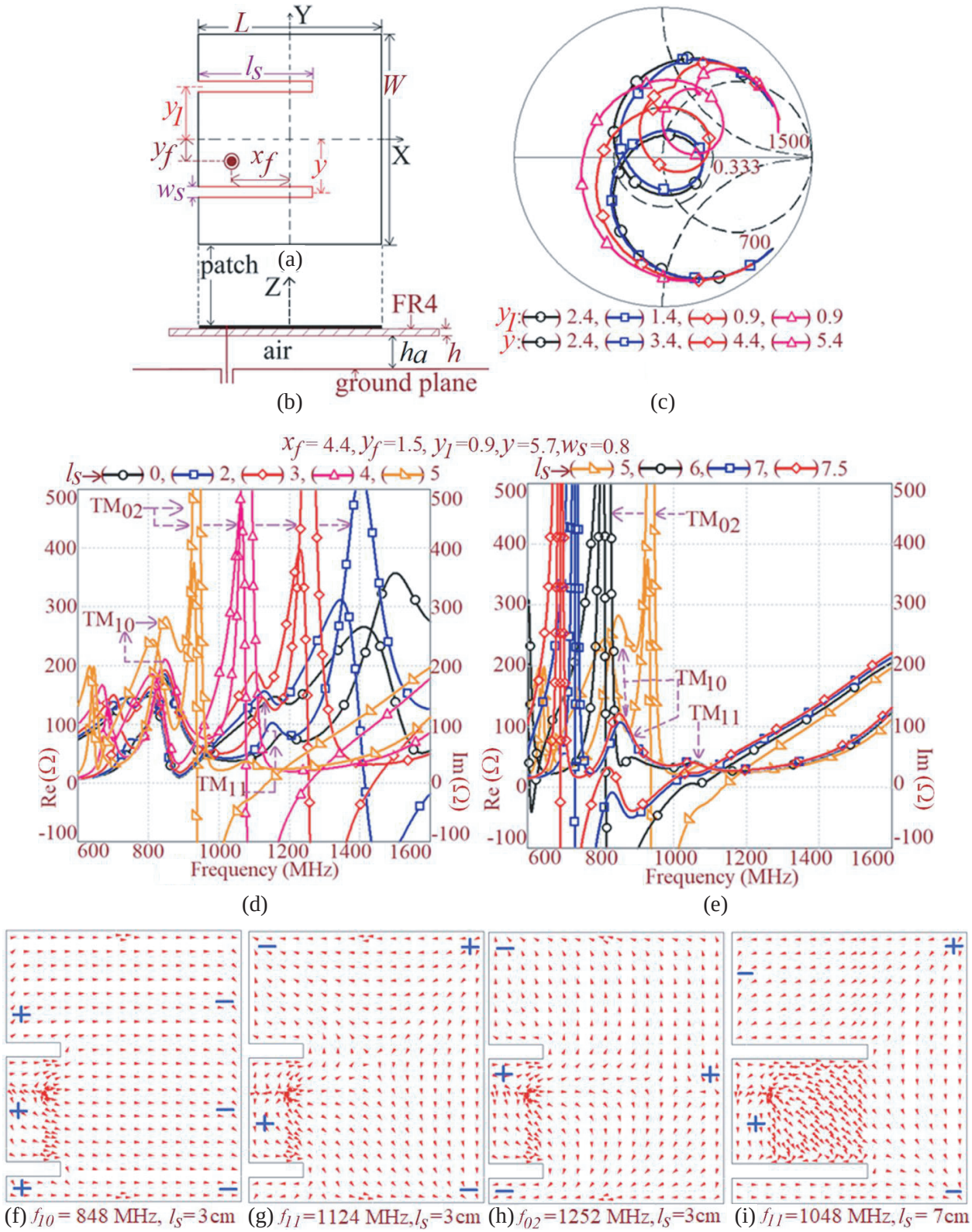

Figure 1. (a), (b) E-shape MSA, its (c) smith chart for varying y_1 & y ($l_s = 8.5$, $x_f = 3.6$, $y_f = 0$), its (d), (e) resonance curve plots for variation in pair of slot length, and (f)–(i) surface current distribution at the observed resonant modes for coaxially fed offset E-shape MSA.

present. Hence to achieve the wideband response along with the CP response, equal length offset slot cut design of E-shape MSA is explored here. This is because the offset slots will create asymmetry in the structure, which can assist in the excitation of bi-directional currents on the patch to yield the CP characteristics. Therefore, starting with the wideband E-shape MSA, to study the effects of offset slots, y_1 and y are varied, and Smith chart for them is shown in Figure 1(c). Here, y_1 is reduced from 2.4 to 0.9 cm, whereas y is increased from 2.4 to 5.4 cm. To ensure the placement of one of the slots forming the E-shape patch above the coaxial feed, y_1 is not reduced below 0.9 cm. With the variation in y_1 and y, the impedance locus becomes inductive as the loop in the smith chart is formed in the higher inductance region. An increase in the inductive component is attributed to the increase in the patch width as seen by the coaxial feed against the variation in y_1 and y. With a higher separation between the pair of slots, an additional smaller size loop is observed in the impedance locus. A larger loop in the smith chart corresponds to the initial wideband response. To explore the variation in AR values across the two loops and the resonant modes contributing to them, a detailed parametric study is carried out. The slot length l_s is increased in steps, and resonance curve plots and surface current distributions at the observed resonant modes are shown in Figures 1(d)–(i).

For $y_1 = 0.9$ and $y = 5.7$ cm, with an increase in l_s, TM_{02} and TM_{11} mode frequencies decrease, whereas TM_{10} mode frequency remains constant. The surface currents at TM_{02} and TM_{11} modes are orthogonal to the slot length increment. This elongates their resonant current path length that reduces their frequency. It can be noted that reduction in TM_{02} mode frequency is higher than the reduction at TM_{11} mode frequency. This is attributed to the two half wavelength variations at TM_{02} mode against a single half wavelength variation at TM_{11} mode, present along the patch width where the pair of offset slots are present. For $l_s > 5$ cm, TM_{02} mode frequency decreases below TM_{10} mode frequency, whereas marginal variations in TM_{11} mode frequency is observed. For $l_s > 5$ cm, surface current distribution at TM_{10} mode remains along the patch length, but at modified TM_{11} mode, current components are bi-directional. This leads to the AR value below 3 dB near the 1050 MHz frequency, i.e., near the modified TM_{11} mode. However, an appropriate impedance matching at TM_{10} and TM_{11} modes together is only obtained for $l_s > 7.0$ cm. The wideband and CP response also depends upon the input impedance at the respective resonant modes. Therefore, the parametric study was carried out for the variation in y_f, whose plots are shown in Figures 2(a) and (b). With the decrease in y_f input impedance at TM_{10} mode marginally changes whereas at modified TM_{11} mode, it increases. Although a minimum value of AR near the modified TM_{11} mode frequency does not change, this variation leads to a wider AR curve that yields optimum result. Thus using this procedure, an offset slots E-shape MSA is optimized for

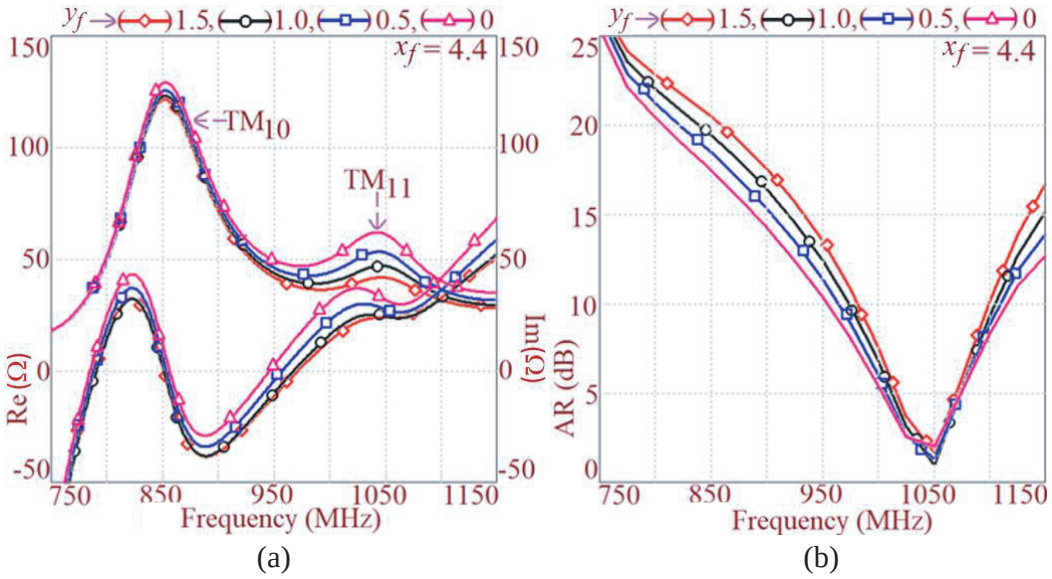

Figure 2. (a) Resonance curve and (b) AR plots against variation in y_f for coaxially fed offset slots cut E-shape MSA.

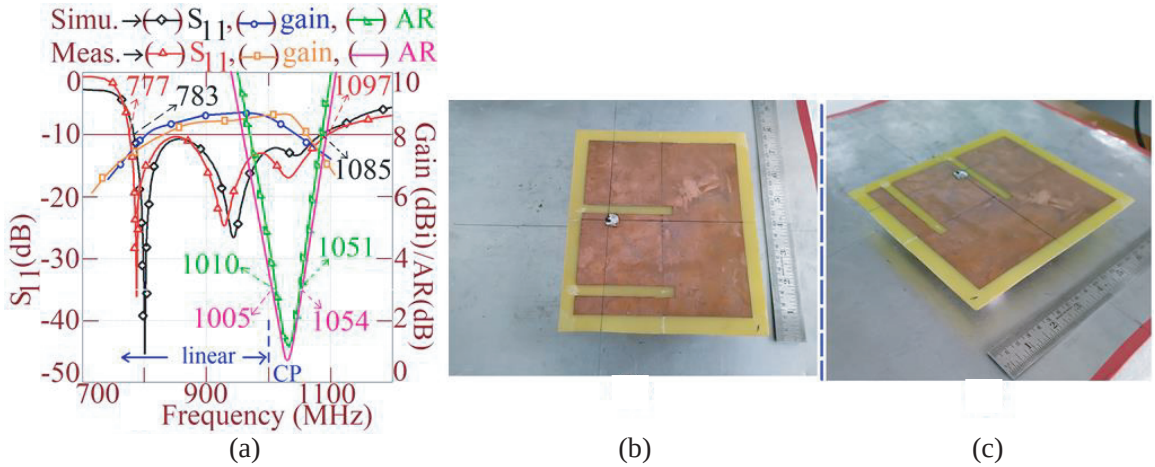

Figure 3. (a) S_{11}, AR and gain plots over the BW and (b), (c) fabricated prototype for coaxially fed offset E-shape MSA, ($L = 13$, $W = 15$, $l_s = 7.4$, $x_f = 4.4$, $w_s = 0.8$, $y_1 = 0.9$, $y = 5.7$ cm).

the wideband and CP response, and results for them are shown in Figure 3(a). The impedance BWs in the simulation and measurement for $S_{11} < -10$ dB are 302 MHz (32.33%) and 320 MHz (34.15%), respectively, with a peak broadside gain of 8.6 dBi.

Towards the higher frequencies of the impedance BW, CP response is observed. Here the simulated and measured values of the CP BW for AR less than 3 dB are 41 MHz (3.9%) and 49 MHz (4.7%),

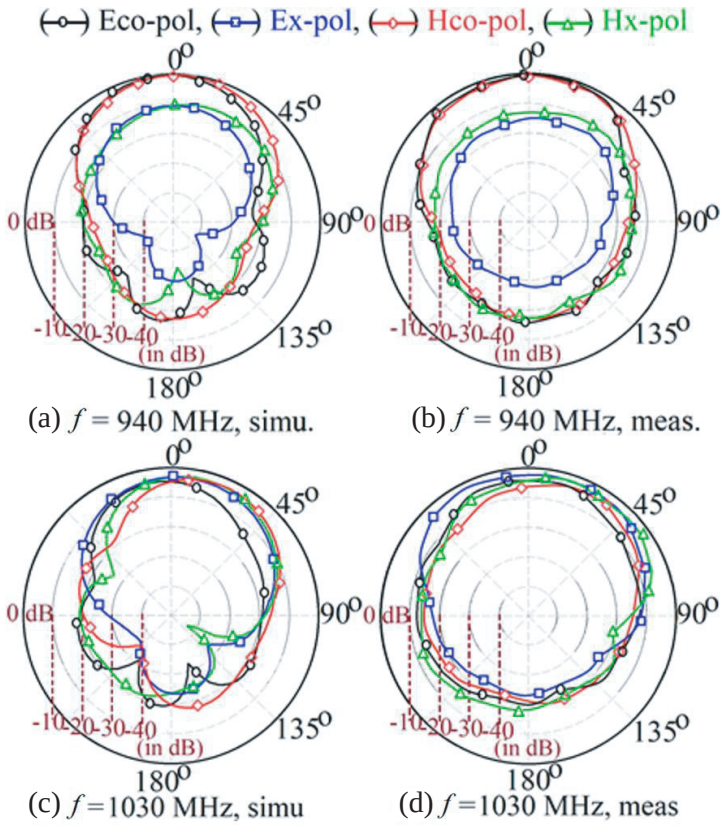

Figure 4. Radiation pattern at the center frequency of (a), (b) wideband and (c), (d) CP response for coaxially fed offset slots cut E-shape MSA.

respectively. The fabricated antenna is shown in Figures 3(b) and (c). The radiation pattern plots near the center frequency of the wideband and CP response are shown in Figures 4(a)–(d). In the proposed design, in the initial range of S_{11} BW, TM_{10} mode is dominant. Therefore, in this frequency range antenna exhibits LP response which is referred to as the wideband region, as shown in Figure 3(a). Towards the higher frequencies of the BW, TM_{11} mode is present. This leads to a CP response with AR values reduced below 3 dB. This is shown as a CP region in the S_{11} plot, as mentioned in Figure 3(a).

Over the entire wideband frequency range, the radiation pattern is in the broadside direction with an E-plane aligned along $\Phi = 0$. Over the wideband response, the difference between the co and cross polar levels is more than 10–15 dB. In the CP band, at the center frequency of the AR BW, the pattern is in the broadside direction with co and cross polar levels within 3 dB difference, which represents the CP radiated fields. The CP response is further confirmed by observing the time varying surface current distribution at the center frequency of the AR BW as shown in Figures 5(a)–(d) and the simulated polarization plot as shown in Figure 5(e). The time varying surface currents rotate in an anticlockwise direction, thereby realizing the right hand CP (RHCP) response. In the simulated polarization plot at the same frequency, RHCP field components are dominant. The sense of rotation is experimentally verified by using a nearly square MSA (SMSA) as a transmitter antenna, which is excited either in left hand CP (LHCP) or RHCP wave. The maximum power is received when the sense of rotation of the transmitter antenna matches the receiver antenna (proposed MSA). For the LHCP excitation of the transmitter, received power at the antenna under test decreases by 8–10 dB. This experimentally confirms the sense of rotation of the CP wave.

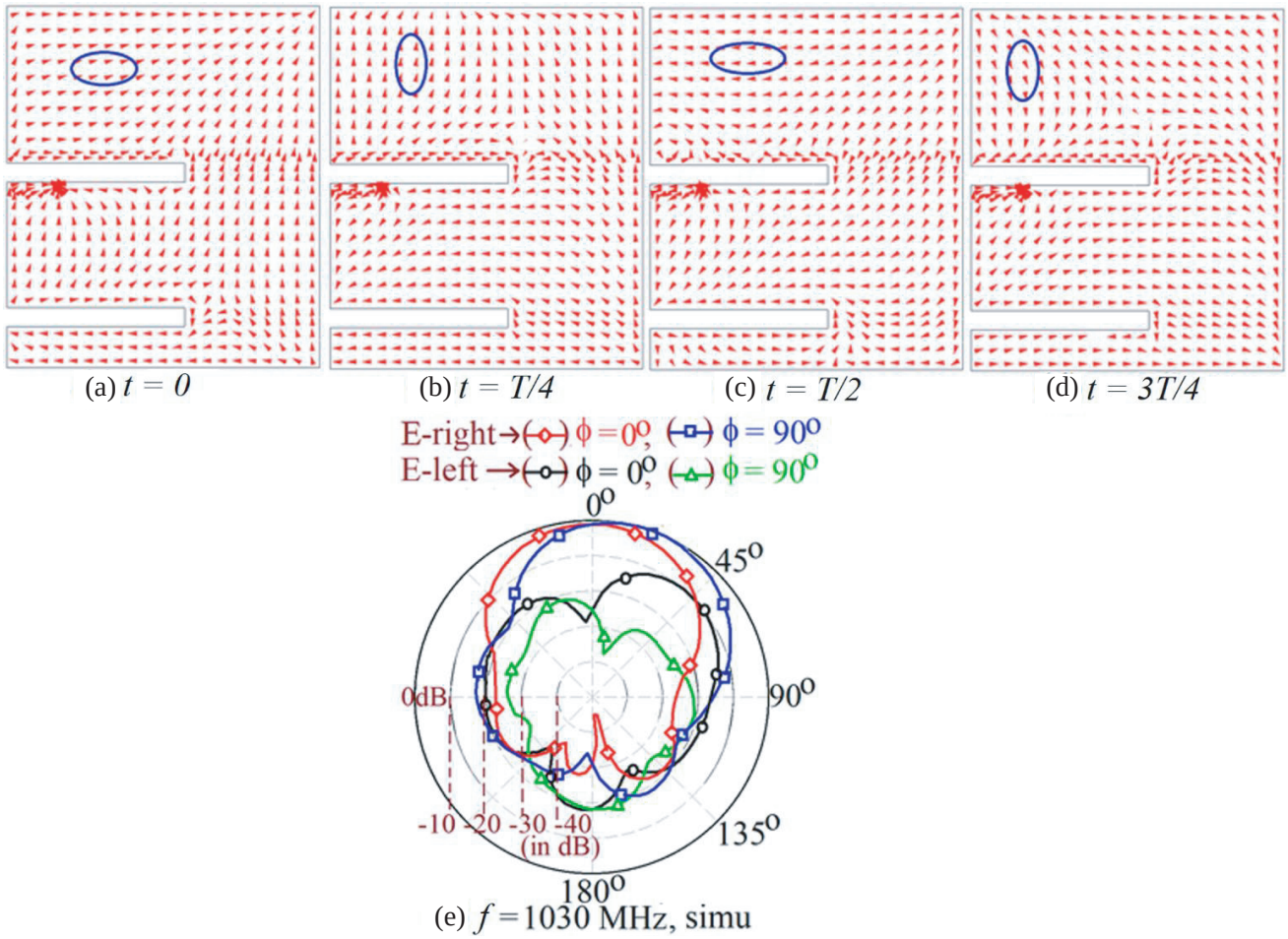

Figure 5. (a)–(d) Time varying surface current distribution, (e) polarization plot at the center frequency of the CP BW for coaxially fed offset slots cut E-shape MSA.

3. HALF E-SHAPE MSAS FOR WIDEBAND & CP RESPONSE

By using the symmetry of E-shape MSA across the coaxial feed, a compact design of half E-shape MSA is reported that yields impedance BW of 20% [15]. In this compact design, patch width is smaller than its length, and thus it yields LP response. The design of modified half E-shape employing a nearly SMSA is reported in [35]. In this design, a shorting bar is used that converts the wideband half E-shape patch into a CP design. But in this design, CP band lies inside the VSWR BW, and thus the two spectrums are not separate. Further to convert from LP to CP characteristics, additional shorting bar is needed. Instead of this complex design approach, a novel design of half E-shape MSA is proposed here for the wideband and CP response, which employs a simple rectangular slot as shown in Figure 6(a). The equivalent SMSA is designed on an FR4 substrate that is suspended in air above the ground plane for $h_a = 2$ cm. Thus for the total substrate thickness of 2.16 cm, the side length of SMSA is parametrically optimized using IE3D software for the fundamental mode frequency of 900 MHz. For this frequency, L is found to be 13 cm. The reported design of half E-shape MSA offers wideband LP response as the patch width is less than its length [15]. Hence, a square patch is selected in the proposed design as it will help in strengthening the bi-directional current variations over the slot cut patch, which can yield CP response in addition to the wideband response. To analyze the effects of rectangular slot length, the parametric study was carried out. For the coaxial feed at $x_f = 3.1$ & $y_f = 1.0$ cm, and slot parameters as $w_s = 2.8$, $y_1 = 3.5$ cm, resonance curve plots for the increase in l_s and surface current distribution at the observed resonant modes for $l_s = 4.0$ cm are shown in Figures 6(b)–(f). As the square patch is present, TM_{10} and TM_{01} mode frequencies are equal. Therefore for $l_s < 2$ cm, a single resonant peak is observed. At this single peak, surface currents vary along the patch diagonal length. As noted

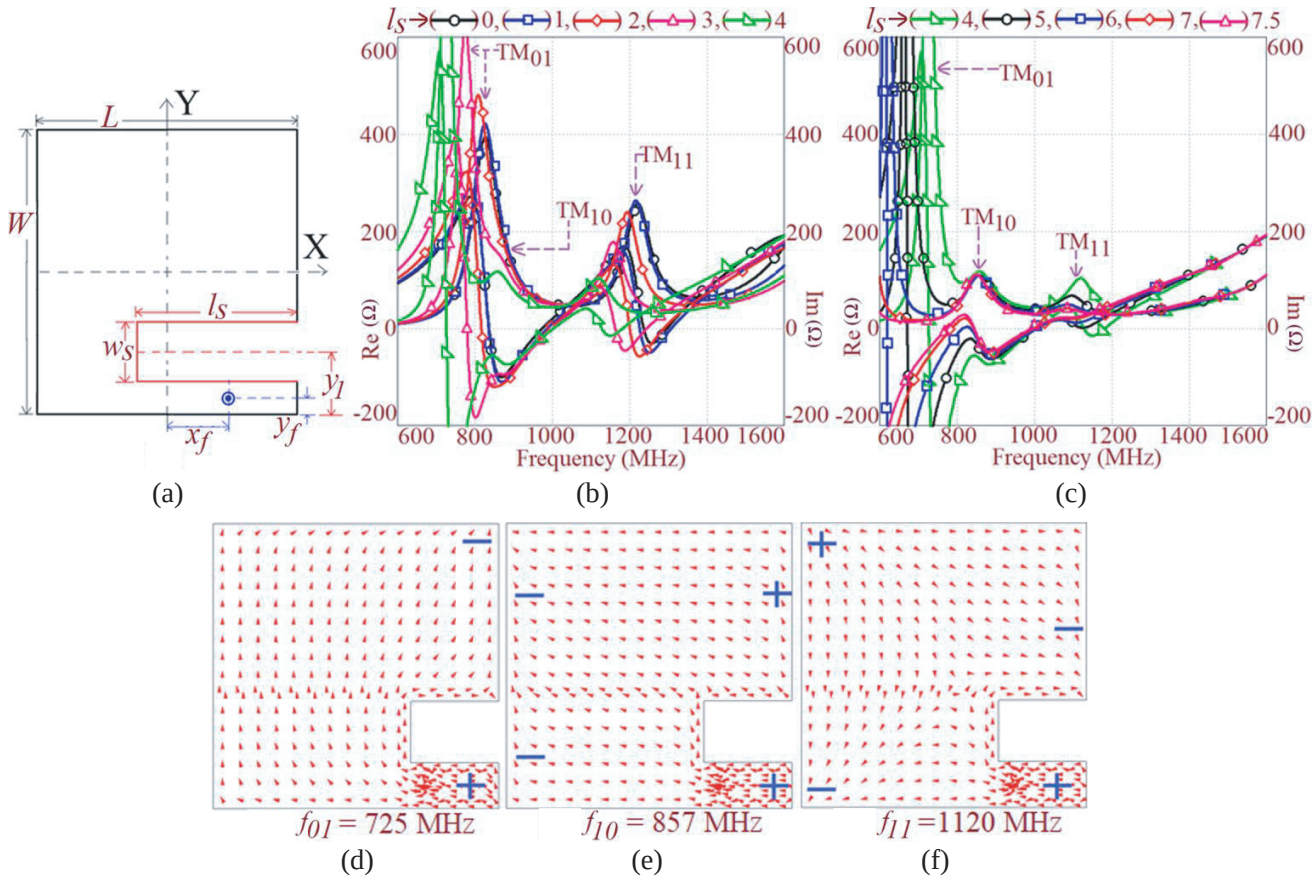

Figure 6. (a) Half E-shape MSA, its (b), (c) resonance curve plots for variation in slot length, (d)–(f) surface current distribution at observed resonant modes for Half E-shape MSA for $l_s = 4$ cm.

from the current distribution plot, next resonant peak is due to TM_{11} mode. With an increase in the slot length above 2 cm, TM_{01} mode frequency decreases, and TM_{10} mode frequency remains constant. With this two isolated resonant peaks are observed in the resonance curve plot. Further for $l_s > 5$ cm, TM_{10} mode frequency remains constant, whereas TM_{11} mode frequency shows smaller reduction in its value. The surface currents at TM_{10} mode remain along the patch length whereas at TM_{11} mode, they are bi-directional. This yields AR value less than 3 dB near the modified TM_{11} mode frequency. The impedance at TM_{10} and modified TM_{11} mode remains below 100 Ω to yield frequency response for $S_{11} < -10$ dB. Thus, the slot length yields the tuning in between TM_{10} and TM_{11} mode frequencies that yields wideband response due to the TM_{10} mode and a CP response due to the modified TM_{11} mode. The effects of variation in slot position y_1 and slot width w_s were also studied. On either side of the respective parameter values selected as above, the impedance and AR BW degrade.

Thus, an optimum response is obtained for the antenna parameters as provided below, and the simulated and measured results are shown in Figure 7(a). The simulated and measured S_{11} BWs of 350 MHz (37.1%) and 367 MHz (38.9%), respectively with a peak broadside gain of above 8 dBi, are achieved. Towards the higher frequency range of the BW, the antenna shows CP response. Here, the simulated and measured values of the AR BW are 48 MHz (4.5%) and 56 MHz (5.3%), respectively. In this design, maximum of the gain and AR BW is present along $\theta = 15°$ & $\Phi = 0°$. The direction of maximum away from broadside direction is attributed to a single slot cut design that makes the design asymmetric with respect to coaxial feed point, which is unlike the E-shape design. The radiation pattern plots near the center frequencies of the impedance and AR BW are shown in Figures 7(b)–(e). The broadside radiation patterns are observed over the impedance and AR BW. Over the wideband response, the E-plane is aligned along $\Phi = 0°$. Over the initial wideband region, antenna shows cross polar levels less than 10 dB. They are higher than that present in the wideband offset E-shape MSA,

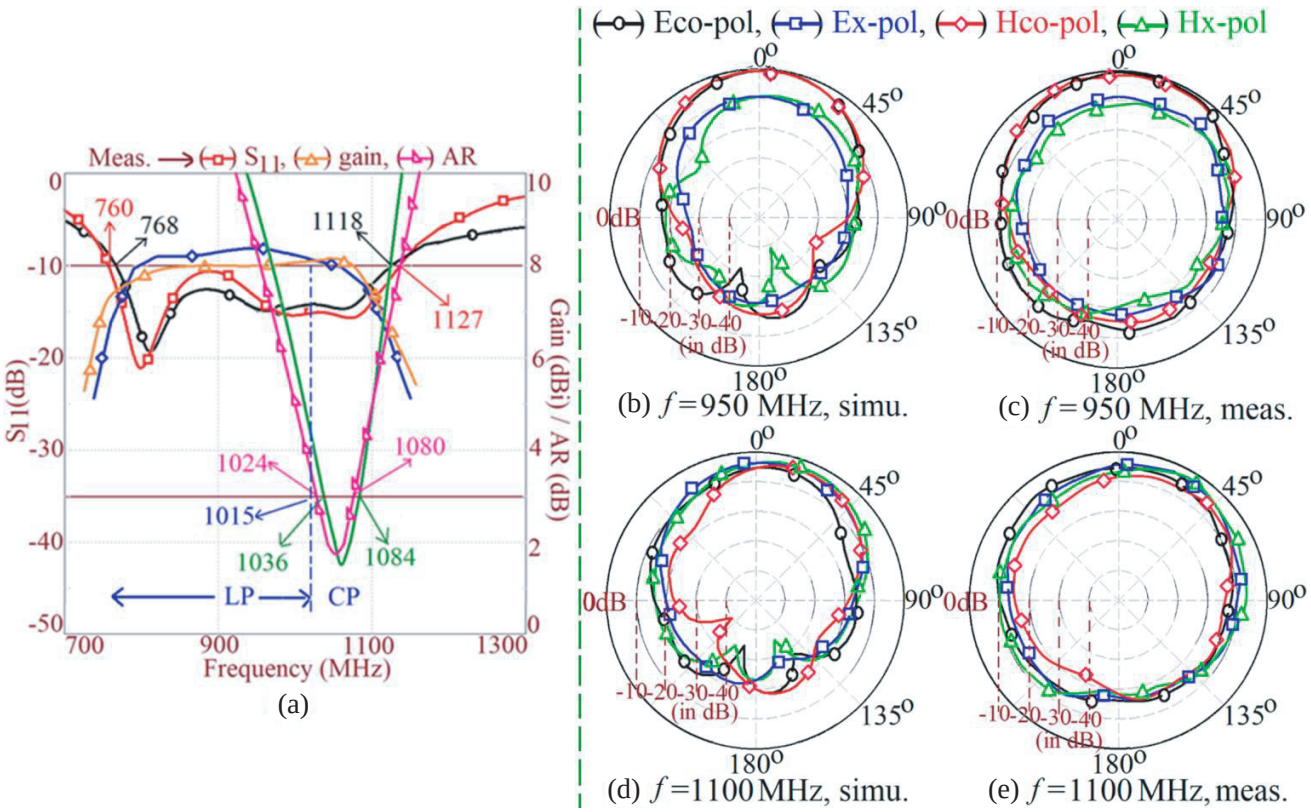

Figure 7. (a) S_{11}, Gain and AR BW plots, and radiation patterns at the center frequency of (b), (c) wideband and (d), (e) CP response for coaxially fed Half E-shape MSA, ($L = 13$, $l_s = 7.4$, $w_s = 2.8$, $y1 = 3.5$, $x_f = 3.1$, $y_f = 1.0$ cm).

mentioned above. This is attributed to the single slot design that makes the configuration asymmetric with respect to the coaxial feed axis. At the center frequency of the AR BW, radiation pattern remains in the broadside direction. However due to the CP response, the difference between the co and cross polar levels is less than 3 dB. The time varying surface current distribution at the center frequency of the AR BW is shown in Figures 8(a)–(d). Here the currents rotate in clockwise direction indicating the LHCP response. This is also confirmed from the simulated polarization plots shown in Figure 8(e), wherein the left-hand field components are dominant. The sense of rotation is also confirmed in the lab using CP SMSA excited in either LHCP or RHCP. For the LHCP excitation of the transmitter antenna, received signal strength is maximum. The fabricated prototype of the antenna is shown in Figure 8(f). In the above configurations, coaxially fed half E-shape MSA is optimized on the total substrate thickness of 2.16 cm, i.e., $0.07\lambda_g$ in thickness. This value is calculated with reference to 950 MHz, which is the center frequency of the S_{11} BW. The thicker substrate needs longer probe length that increases the spurious radiation from the probe in the end-fire direction. The thicker substrate also supports the surface wave excitation. To reduce the probe length (substrate thickness), two techniques are explored as discussed in the following section.

4. MODIFIED GROUND PLANE AND BEVELED FEED DESIGNS OF E-SHAPE MSAS

The designs of coaxially fed E-shape and half E-shape MSAs backed by bow-tie shape ground plane are shown in Figures 8(g)–(i). In these designs, MSA is fabricated in three layers suspended configuration in which two layers of FR4 substrate are separated by an air gap of h_a cm. On the bottom FR4 layer, modified ground plane is present whereas on the top layer, patch exists. The total substrate thickness $(2h + h_a)$ is selected to be 2.22 cm, which is nearly the same as that present in the above design. The use of bow-tie shape ground plane is discussed in [38] for proximity fed MSA, to enhance the impedance BW on lower substrate thickness. The same is explored here in coaxially fed wideband and CP MSAs to reduce the substrate thickness. In both the configurations, parametric study for the reduction in air gap h_a and increase in bow-tie ground plane parameter d is carried out. The effects of these parametric variations are described in [38], hence they are not presented here. For smaller h_a, an increase in d yields impedance matching for the loop position inside VSWR = 2 circle to achieve the optimum result. Using the bow-tie shape of the ground plane, antenna broadside gain decreases. Thus, an optimum configuration in the two designs is considered as the one for which substantial amount of BW increase supported with reduction in h_a is achieved for the broadside gain reduction around 1.5 dBi. Based on this, results for the optimum design are presented in Figures 9(a)–(c). In offset slot cut E-shape MSA design, simulated and measured impedance BWs are 412 MHz (47.57%) and 415 MHz (48.39%), respectively. Simulated and measured AR BWs towards the higher frequency region of the impedance BW are 47 MHz (4.49%) and 45 MHz (4.37%), respectively. The peak broadside gain is 6.1 dBi. On square ground plane and substrate thickness of 2.22 cm ($0.07\lambda_g$), offset E-shape MSA yields impedance and AR BW of 272 MHz (29.44%) and 37 MHz (3.62%), respectively with a peak gain of 7.7 dBi.

These values are smaller than the above offset slot cut design employing substrate thickness of 2.16 cm. This is attributed to the three layer suspended design employed in modified ground plane MSA, which has larger value of effective dielectric constant of the antenna cavity. Against the conventional ground plane, E-shape design using bow-tie shape ground plane offers more than 15% impedance BW and a higher AR BW, but on substrate thickness of $0.037\lambda_g$. Against the E-shape MSA design for thickness of 2.16 cm, modified ground plane design offers 12% increase in the impedance BW with a smaller increase in AR BW as well, but with $0.03\lambda_g$ reduction in total substrate thickness. Due to the bow-tie nature of the ground plane, peak gain decreases by around 1.5–1.8 dBi. The half E-shape MSA using bow-tie shape ground plane on the total substrate thickness of 1.62 cm ($0.052\lambda_g$) yields simulated and measured impedance BWs of 515 MHz (55.23%) and 523 MHz (56.63%), respectively. The simulated and measured AR BWs are 21 MHz (1.96%) and 19 MHz (1.8%), respectively. In this design, peak broadside gain is 5.0 dBi. In comparison with the design using the thickness of 2.16 cm ($0.07\lambda_g$), bow-tie ground plane design offers 15% increase in the total impedance BW with $0.02\lambda_g$ reduction in the total substrate thickness. But in this design, the AR BW has decreased, and broadside gain shows variation in values across the impedance and AR BW. This gain variation is attributed to

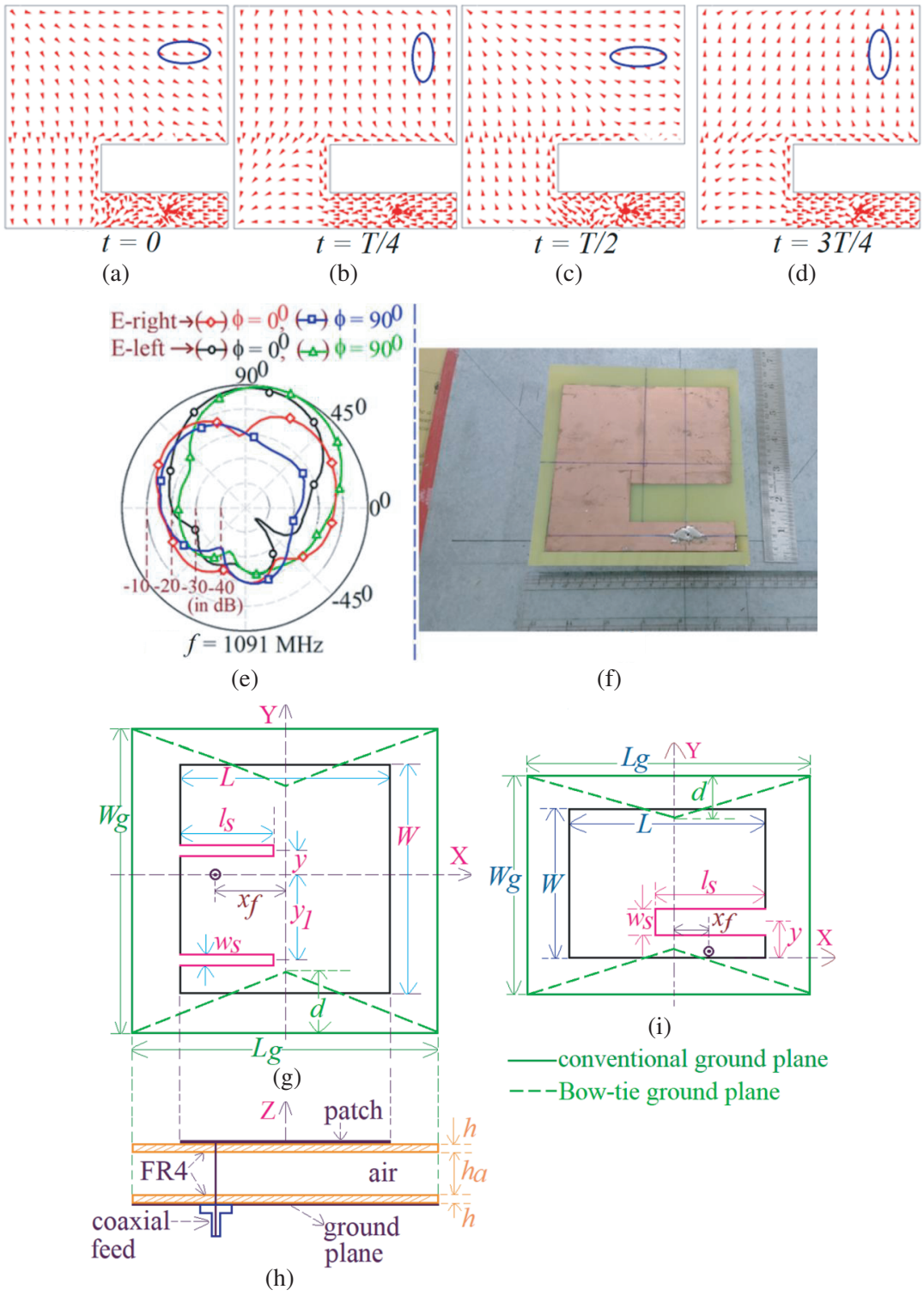

Figure 8. Simulated (a)–(d) time varying surface current distribution, and (e) polarization plot at the center frequency of CP BW and (f) fabricated prototype for coaxially fed half E-shape MSA, designs of (g), (h) E-shape and (i) half E-shape MSA backed by Bow-tie shape ground plane.

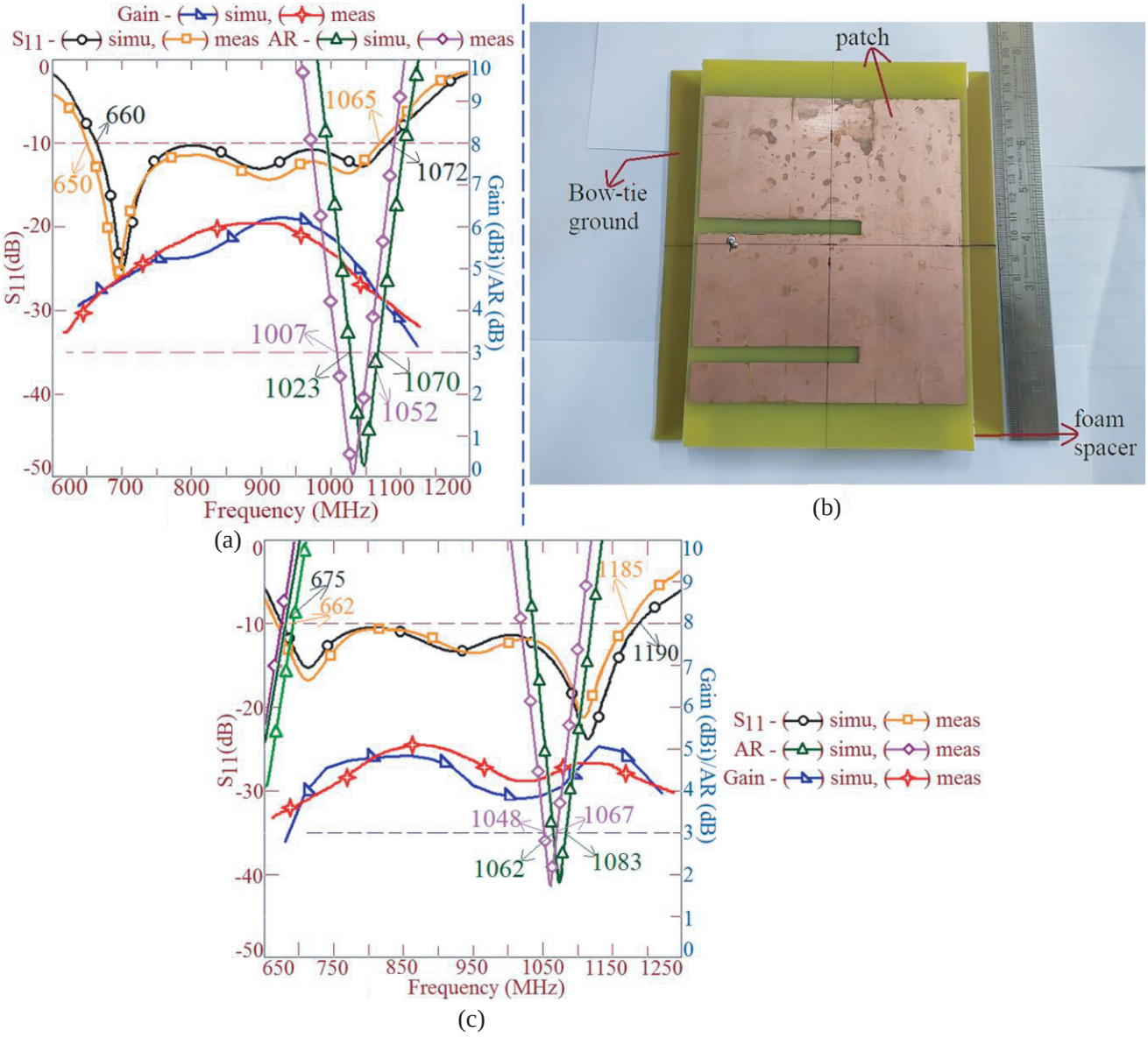

Figure 9. (a) S_{11}, AR and gain plots for offset E-shape MSA backed by Bow-tie shape ground plane and its (b) fabricated prototype ($L = 13$, $h = 0.16$, $h_a = 0.9$, $l_s = 8.0$, $x_f = 4.8$, $w_s = 0.8$, $y_1 = 0.9$, $y = 5.7$, $d = 4.5$ cm), (c) S_{11}, AR and gain plots for half E-shape MSA backed by Bow-tie shape ground plane ($L = 13$, $h = 0.16$, $h_a = 1.3$, $l_s = 9.8$, $x_f = 3.9$, $y_f = 1.0$, $w_s = 2.8$, $y_1 = 3.9$, $d = 4.0$ cm).

the asymmetrical nature of the configuration with respect to the bow-tie shape ground plane.

To remove this asymmetry in half E-shape MSA design, a modified beveled coaxial feeding using conventional ground plane is employed as shown in Figures 10(a) and (b). In this design, air suspended configuration as mentioned in Figure 1(b) is considered. Using bow-tie shape ground plane only, the three layer suspended design is considered, as it offers simplicity in implementing modified ground plane profile on the bottom FR4 layer. The beveled feed section consists of tapered width bend section, with width L_t on the patch side and L_b at the bottom side that connects to the coaxial probe. On the total substrate thickness of 2.16 cm ($h_a = 2.0$ cm), using the parametric optimization, various antenna parameters for the wideband response are optimized, and they are provided below in Figure 10. The feeding strip is placed below the patch at a height of $h_s = 0.7$ cm ($0.022\lambda_g$). The working of the antenna in terms of resonant modes is similar to that of the coaxially fed half E-shape MSA design.

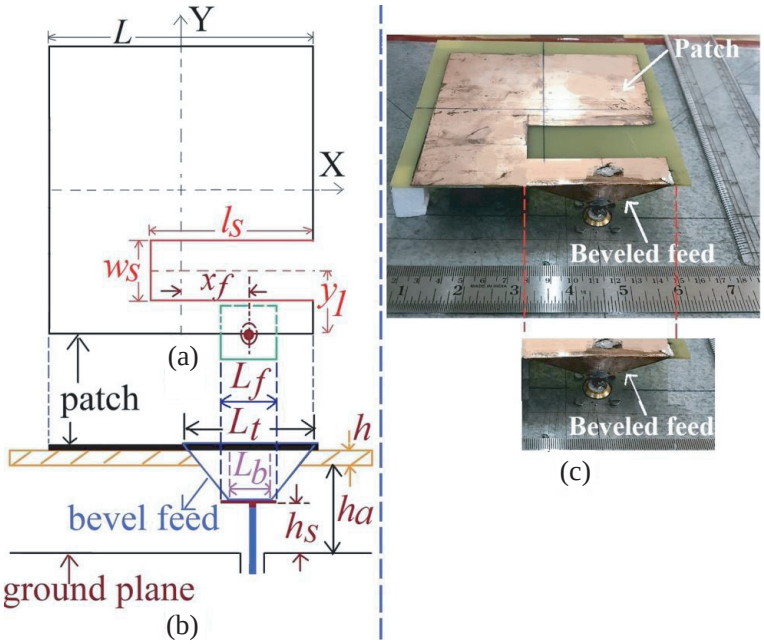

Figure 10. (a), (b) Modified beveled fed half E-shape MSA and its (c) fabricated prototype, ($h_a = 2.0$, $L_t = 7.4$, $L_b = 0.36$, $L_f = 0.6$, $h_s = 0.7$, $x_f = 2.8$, $l_s = 7.4$, $w_s = 2.8$, $y_1 = 3.5$ cm).

Thus here the simulated and measured S_{11} BWs of 384 MHz (40.17%) and 401 MHz (41.1%) with a peak broadside gain of 8.4 dBi are obtained. The simulated and measured values of the AR BWs are 55 MHz (5.14%) and 51 MHz (5.2%), respectively. This antenna exhibits similar radiation pattern and gain characteristics over the S_{11} and CP BW to that present in the design of coaxially fed half E-shape MSA. Thus using beveled feeding, for the feed probe length of $0.022\lambda_g$ improved values of AR BW and gain are obtained. The fabricated prototype of the antenna is shown in Figure 10(c). Due to the geometrical difference of the offset E-shape MSA against the half E-shape MSA, beveled feed design is complex to implement, hence not studied here.

5. DESIGN METHODOLOGY FOR MODIFIED E-SHAPE AND HALF E-SHAPE MSAS

The wideband and CP response in the proposed modified E-shape variations is due to the modified TM_{10} and TM_{11} resonant modes. By extensively studying the surface current distribution at the patch resonant modes, formulation in their lengths is proposed here. In the offset slots cut E-shape design, against the slot length increment, TM_{02} and TM_{11} mode frequencies decrease whereas TM_{10} mode frequency remains constant. By analyzing the variations in current paths at each mode, resonant length is formulated. At TM_{10} mode, a pair of slots does not perturb the current path length, and thus its formulation is obtained by using Equation (1). At TM_{02} mode, the surface currents show two half wavelength variation along the patch width. Due to the presence of a pair of slots, the current path length increases as modal current components circulate around the slot lengths. The perturbation in resonant length depends upon the slot length as a function of the patch length. Based upon these observations, resonant length at TM_{02} mode is formulated by using Equation (3). At TM_{11} mode, the currents vary along the patch length and width. The modal current components along the patch length are not modified in their length. However, along the width they are modified in their length as the current vectors circulate around the slot length. Thus the modified patch width at TM_{11} mode is obtained by using Equation (4). An effective length and width for calculating the TM_{11} mode frequency are obtained by using Equations (1) and (4), respectively. The frequency at the three modes is calculated by using Equation (5), and % error between the calculated and simulated frequencies is

obtained by using Equation (6). At the three modes, a close matching between the calculated and simulated frequencies with % error less than 3% is obtained.

For offset E-shape MSA,

$$L_e = L + (1.8h_t/\sqrt{\varepsilon_{re}}), \quad \text{TM}_{10} \text{ mode} \tag{1}$$

$$\varepsilon_{re} = \varepsilon_r (h + h_a)/\varepsilon_r h_a + h \tag{2}$$

$$W_e = W + (4l_s)(1.5l_s/L) + (2h_t/\sqrt{\varepsilon_{re}}), \quad \text{TM}_{02} \text{ mode} \tag{3}$$

$$W_e = W + (2l_s)(l_s/1.2L) + (2h_t/\sqrt{\varepsilon_{re}}), \quad \text{TM}_{11} \text{ mode} \tag{4}$$

$$f_{mn} = c/2\sqrt{\varepsilon_{re}} \left(\sqrt{(m/L_e)^2 + (n/W_e)^2} \right) \tag{5}$$

$$\%\text{Error} = |f_{cal} - f_{ie3d}/f_{ie3d}| \times 100 \tag{6}$$

In half E-shape MSA, the wideband and CP response is realized due to the optimum separation between TM_{01}, TM_{10}, and TM_{11} resonant modes. The TM_{10} mode frequency marginally changes against the slot length, and its formulation is given by Equation (1). The surface currents at TM_{01} mode circulate around the slot lengths, and perturbation in them modifies the patch width, as given in Equation (7). At TM_{11} mode, current varies along the patch length and width, of which current components only along the patch width are modified in their length. Thus the modified patch length and width at TM_{11} mode are given by using Equations (1) and (4), respectively. The frequency at each mode is calculated by using Equation (5) and % error by using Equation (6). At the three modes, a close matching between the two frequencies is observed with % error less than 3%.

$$W_e = W + (2l_s)(1.2l_s/L) + (1.8h_t/\sqrt{\varepsilon_{re}}), \quad \text{TM}_{01} \text{ mode} \tag{7}$$

Using the above formulation, a design methodology to realize similar antennas at other frequencies is presented here. For this, the center frequency of the CP band f_{cp} is specified. Although the CP band lies near the modified TM_{11} mode frequency, this frequency cannot be used to calculate the patch dimensions directly since the modified frequency includes slot effect. As noted from the resonance curve plots in both the designs, the TM_{10} mode frequency remains constant against the slot length variations. Therefore, by using Equation (8), the TM_{10} mode frequency for the given f_{cp} is calculated. This frequency ratio is selected based upon the ratio present in between the TM_{10} and f_{cp} values, in the optimum design above. Similar to the above design, the total substrate thickness h_t for the redesigned MSA is selected as per Equation (9). For calculating h_t, initial value of the effective dielectric constant (ε_{re}) is required to be known. However, it is not available since it depends upon air gap h_a present in the suspended design. Therefore, an initial approximation of 1.06 is assumed. This assumption is based upon the value of ε_{re} as calculated in the original design above. Further from the value of h_t as calculated from (9), practically realizable value of h_a is selected. Using this value, ε_{re} is recalculated. The new value of ε_{re} marginally differs from the initial assumption. This iterative process is carried out once since the initial ε_{re} value is unknown. In further calculations, a new value of ε_{re} is considered. The RMSA length for the given TM_{10} mode frequency is calculated by using Equation (10). The RMSA width W is selected as $1.154L$, and the coaxial feed is placed at a distance of $0.338L$ from the origin, along the x-axis. The two slots of width $0.053W$ are placed at a distance of $y_1 = 0.06\,\text{W}$ and $y = 0.38W$, on either side of the feed axis. These values are selected to be the same as that present in the original design above.

$$f_{10} = f_{cp}/1.24 \tag{8}$$

$$h_t = 0.063\,(30/f_{10}\sqrt{\varepsilon_{re}}) \tag{9}$$

$$L = (30/f_{10}\sqrt{\varepsilon_{re}})\,(1.8h_t/\sqrt{\varepsilon_{re}}) \tag{10}$$

The unique design feature in the proposed offset E-shape MSA as against the reported E-shape variations is that it provides separate operating bands for linearly (wideband) and circularly polarized responses, in the same impedance BW. One such application that requires this kind of pattern response is antennas used in GSM, 900 MHz and GPS L5, 1178 MHz frequency bands. The GSM band can operate with antenna offering wideband response with cross polar levels in the range of 10–15 dB below the co-polar levels, whereas GPS L5 band will require CP response. Thus to cover these two applications, a design procedure is presented here for offset slots cut E-shape MSA for $f_{cp} = 1178\,\text{MHz}$. At this frequency, for

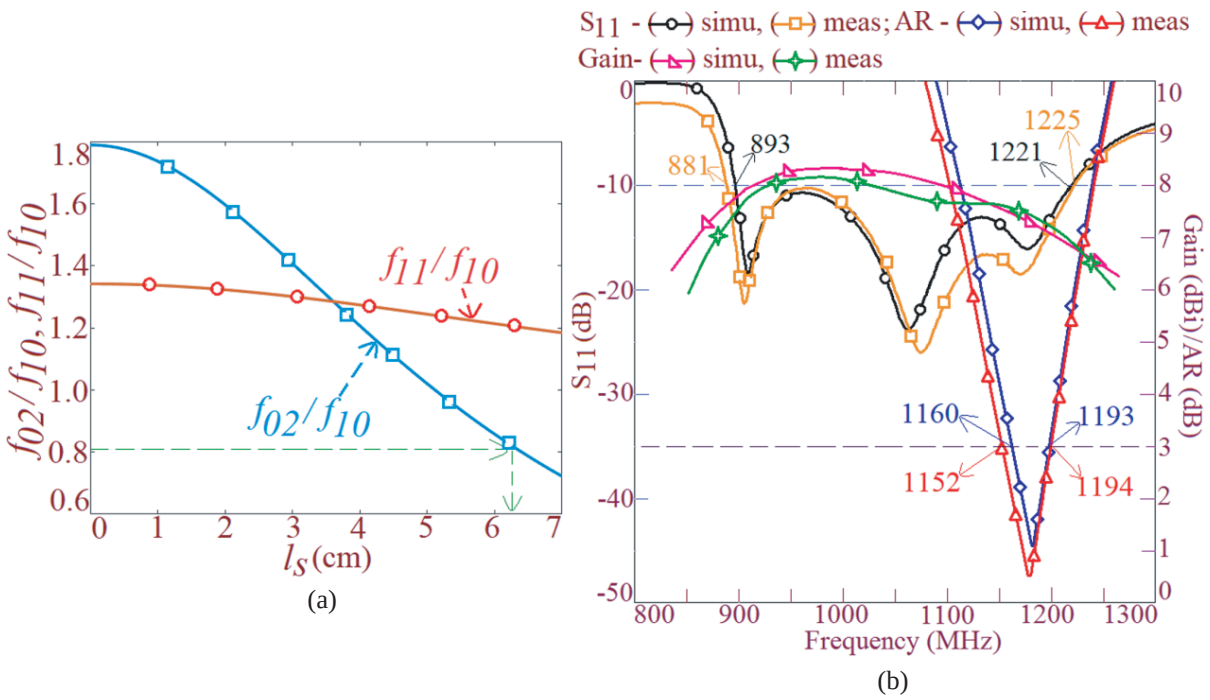

Figure 11. (a) Frequency ratio plots and (b) optimum results for wideband and CP design of offset slots cut E-shape MSA for $f_{cp} = 1178$ MHz, ($h_a = 1.7$, $L = 11.7$, $W = 13.5$, $w_s = 0.7$, $y_1 = 0.8$, $y = 5.1$, $x_f = 3.95$ cm).

the various patch parameters calculated using the above procedure, the resonant length formulation for TM_{10}, TM_{02}, and TM_{11} modes is used to calculate the respective frequencies against the increasing slot length l_s. The ratio plots amongst them against the slot length increments are shown in Figure 11(a). In an offset E-shape MSA design above, an optimum response is obtained for the frequency ratio f_{02}/f_{10} of 0.815. Using the ratio plots, slot length l_s is selected that gives this frequency ratio, and it is found to be 6.2 cm. Various antenna parameters in the redesign configuration are given below in Figure 11. The antenna is designed using these parameters, and simulated and measured results for the same are shown in Figure 11(b). The simulated and measured values of the impedance BW are 328 MHz (31.03%) and 344 MHz (32.67%), respectively. Towards the higher frequencies of the impedance BW, simulated and measured AR BWs of 33 MHz (2.81%) and 42 MHz (3.6%), respectively, are achieved. The deviation in between the two results is attributed to the errors in maintaining the exact air gap for the substrate parameters in the measurement. The simulated center frequency of the CP BW is 1176.5 MHz that is closer to the initially frequency value chosen. Thus, the redesign configuration covers the requirements of GSM 900 MHz and GPS L5 band in the same impedance BW. The redesigned offset E-shape MSA offers broadside radiation pattern across the impedance and AR BW with a peak gain of above 8 dBi.

$$f_{10} = f_{cp}/1.28 \tag{11}$$

Similarly, the redesign procedure for half E-shape MSA for the wideband and CP response is presented for $f_{cp} = 1178$ MHz. In half E-shape MSA, TM_{10} mode frequency also remains constant against the increment in the slot length. Therefore, the TM_{10} mode frequency of the square patch is related to the desired value of f_{cp} (i.e., center frequency of AR BW), by using Equation (11). The substrate thickness h_t for the given TM_{10} mode frequency is calculated by using Equation (9). With an initial assumption of 1.06 for ε_{re}, h_t is calculated, from which practically realizable value of h_a is selected. This further helps to recalculate the value of ε_{re} using Equation (2), to be used in further calculations. The patch length is calculated by using Equation (10). Since the square patch is present in half E-shape MSA design, $W = L$. The coaxial feed is placed at $x_f = 0.238L$, $y_f = 0.077W$ from the patch origin, as shown in Figure 6(a). The slot is cut at a distance $y_1 = 0.269W$ from the horizontal patch edge, and its width is taken as $w_s = 0.215W$.

For f_{cp} = 1178 MHz, various patch parameters are calculated using the above procedure. The resonant length formulation for TM_{10}, TM_{01}, and TM_{11} modes is used to calculate the respective frequencies against the increasing slot length l_s. The ratio plots amongst them against the slot length increments are shown in Figure 12(a). In the above half E-shape MSA design, an optimum response is obtained for $f_{01}/f_{10} = 0.645$. Using the frequency ratio plots for 1178 MHz, slot length l_s is selected that yields this frequency ratio. Using this procedure, various antenna parameters are calculated for f_{cp} = 1178 MHz, and their values are provided in Figure 12, below. The antenna is simulated, and measurement was carried out. The results for the redesigned antenna are shown in Figure 12(b). The simulated and measured values of the impedance BW are 414 MHz (40%) and 408 MHz (39.84%), respectively. Towards the higher frequencies of the impedance BW, simulated and measured AR BWs of 42 MHz (3.6%) and 40 MHz (3.43%), respectively, are achieved. The simulated center frequency of the CP BW is 1181 MHz, which is near the initially chosen frequency. The proposed antenna covers GSM and GPS L5 band, offering wideband characteristics over the initial range of frequencies and CP response near 1178 MHz, thus satisfying the application requirements. The redesigned half E-shape MSA offers broadside radiation pattern across the impedance and AR BW with a peak broadside gain of above 8 dBi.

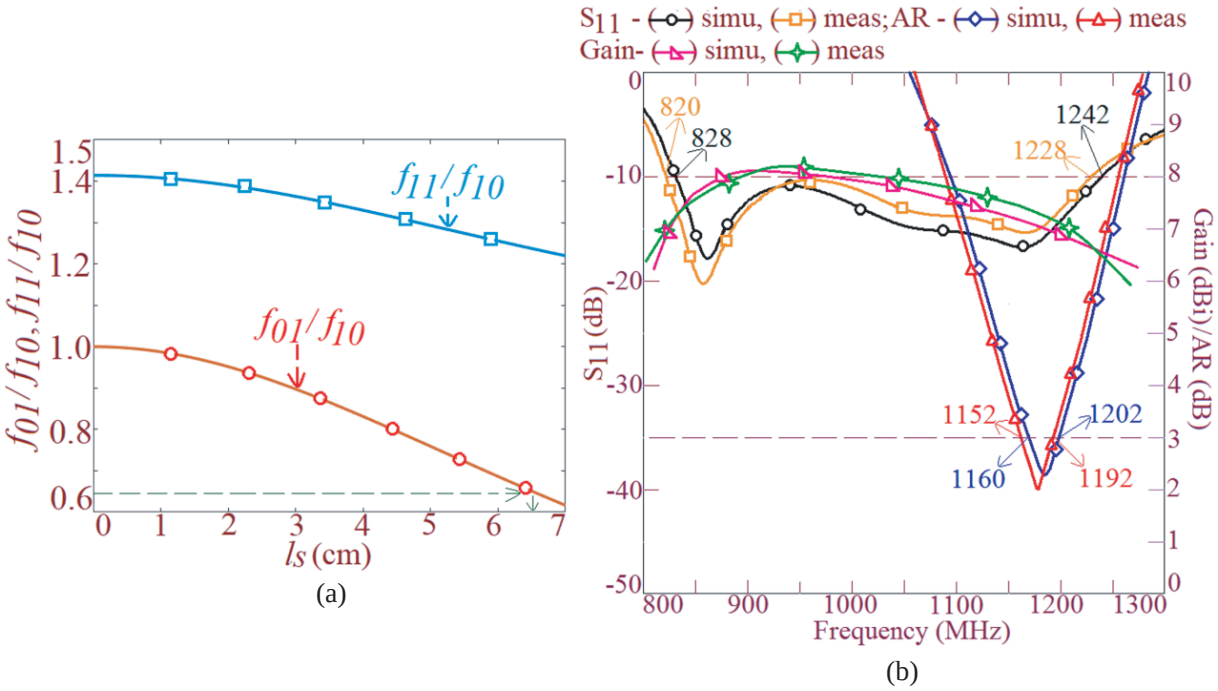

Figure 12. (a) Frequency ratio plots and (b) optimum results for wideband and CP design of half E-shape MSA for f_{cp} = 1180 MHz, (h_a = 1.8, L = 12.0, W = 12.0, l_s = 6.6, w_s = 2.6, y_1 = 3.25, x_f = 2.85, y_f = 0.95 cm).

While the patch parameters are calculated using the proposed formulations in the two designs, non-integer or practically non-realizable values for some of the antenna parameters are obtained. They are rounded off to the nearest possible realizable value. Due to this variation, small deviation in between the simulated frequency values against the targeted value can be observed in the proposed design methodology. Therefore, to achieve the desired frequency band precisely, marginal parametric optimization can be employed in both the configurations. Thus, using the proposed design formulation, variations of E-shape MSAs can be designed with reference to the given CP band frequency, where the wideband linearly polarized response is needed in the adjoining and non-overlapping lower frequency spectrum of the CP response. This is the unique design feature of E-shape MSAs studied in this paper, which is not reported in literature in the wideband and CP E-shape MSA variations. From this design perspective, the configurations presented here are novel and not just the repetitive discussion of widely

reported E-shape MSA. Further, to highlight the new technical contributions in the present study, a detailed comparison for the proposed designs against the reported wideband as well as CP variations is provided in Table 1, below. For the comparison purpose, optimum designs of offset E-shape MSA, half E-shape MSA using conventional ground plane, and offset E-shape MSA using bow-tie shape ground plane are considered, as they offer optimum results in terms of impedance and AR BW, peak gain, and the total substrate thickness, together. The patch area (A_p) and total substrate thickness (h_t), as mentioned in Table 1, are normalized with reference to the wavelength (λ_c) at center frequency of the impedance BW.

Table 1. Comparison of proposed E-shape MSA variations against reported wideband and CP designs.

MSA shown in	Meas. BW (%)	Meas. AR BW (%)	Peak Gain (dBi)	Patch Area (A_p/λ_c)	Substrate thickness (h_t/λ_c)
Fig. 1(a)	**34.15**	**4.75**	**8.7**	**5.8**	**0.069**
Fig. 6(a)	**38.9**	**5.3**	**8.4**	**4.85**	**0.07**
Fig. 8(g)	**48.39**	**4.37**	**6.1**	**5.8**	**0.037**
Ref. [2]	6.8	–	7	0.741	0.04
Ref. [10]	68	–	10	2.244	$0.02\lambda_c$
Ref. [12]	27.2	12.7	–	0.7	0.06
Ref. [13]	13	–	6.5	5.99	.0237
Ref. [19]	78.7	27.5	–	1.6	0.065
Ref. [20]	6.5	13	5	0.293	0.11
Ref. [21]	4.3	0.78	10.3	4.565	0.04
Ref. [22]	2.7	6.3	7	3.56	.035
Ref. [23]	19.5	12.9	9.8	2.4	0.043
Ref. [24]	23	18.9	10.2	4.5	0.048
Ref. [25]	31.7	14.27	7.6	9.2	0.14
Ref. [26]	1.8	0.96	4.73	3.183	0.055
Ref. [27]	38	28.1	8.4	0.628	0.104
Ref. [28]	3.86	0.87	–	3.69	0.025
Ref. [29]	3.1	1.6	5	1.23	0.018
Ref. [31]	9.27	16	8.3	2.34	0.08
Ref. [32]	15.2	3.2	4.5	1.09	0.16
Ref. [35]	35	5.3	–	1.9	0.098

The recently reported modified gap-coupled design of modified rectangular patch in [2] offers more than 5% BW on thinner substrate and by using smaller patch area. However, it does not offer CP characteristics over a portion of the impedance BW. The wideband design using two U-shape slots reported in [10] offers substantially higher BW on a very small substrate thickness. However, this configuration requires differential feeding to offer conical radiation pattern. In addition, it does not provide CP characteristics over a portion of its impedance BW. The wideband configurations reported in [11] offers higher impedance BW but yields only LP response across it. The wideband configurations reported in [12, 13] employ different feedings and yet offer smaller impedance BW. The modified E-shape MSA design, referred to as Ψ-shape patch [14], offers BW greater than 55%. Although here modified higher order modes are present, the antenna does not offer CP response over a small portion of the impedance BW. The CP designs employing thinner substrate as reported in [17, 18] offers smaller AR BW. The design reported in [19] does offer higher AR BW, but the radiation efficiency and hence the gain is poor here as it employs chip resistor loading. The MSA designs reported in [21, 22] offer high gain CP response. However, they employ shorting post to achieve the CP characteristics. Also

the details about which of the shorted patch modes that contributes to the CP characteristics is not explained here. The designs reported in [23–27] require additional patches and power divider circuit to achieve the CP response. The design reported in [28] offers smaller impedance and AR BW, whereas fractal slot cut geometry on the ground plane is complex in designing and offers smaller AR BW [30]. The resonant slot cut CP MSAs reported in [31–36] offers AR BW in the range of 4–5%. However, it lies inside the impedance BW that does not create separate wideband and CP regions. Also the realized impedance BW is smaller here. The characteristics mode-based analysis for the wideband and CP designs employing slots is presented in [16, 37]. This approach does not put forward any design methodology to calculate the patch parameters so as to design the antenna in the specific frequency band. The wideband design using bow-tie shape ground plane as reported in [38] does not offer CP response over the portion of BW, and thus they are unsuitable for applications requiring antenna to function as wideband and CP response in the adjoining spectrums.

In comparison, against the reported slot cut wideband and CP designs, the proposed E-shape MSAs offer higher or comparable impedance and AR BW. It provides a non-overlapping CP region that lies towards the higher frequency of the same impedance BW. This is the main advantage of the proposed designs against the reported resonant slot cut CP designs. This design novelty helps in targeting applications that require antenna to function as a wideband design over a specific frequency range and as a CP design over a certain portion, with no overlapping regions. The design methodology for one such application is mentioned above. Against the reported half E-shape MSA CP design, the proposed configuration is simpler as it does not require additional shorting bar to convert CP to the LP response. Although the AR BW realized in the proposed design is around 3–5%, that lies over the separate frequency spectrum of the total impedance BW. This kind of response is not present in the reported resonant slot cut CP MSAs. The additional TM_{11} mode does add to the impedance BW, but it is spaced separately against TM_{10} mode region where the wideband response is present. In comparison strictly with the wideband slot cut MSA, the proposed design offers similar impedance BW with only LP response, but has additional CP response to follow. Therefore, the proposed designs provide a mixture of LP and CP response but in separate regions. This kind of design feature is not available in the reported slot cut MSAs. An improvement in the antenna BW but on thinner substrate is achieved by using bow-tie shape ground plane profile, and in the design with offset E-shape MSA, it offers more than 12% BW improvement for $0.03\lambda_g$ reduction in the substrate thickness. These values are significant on a thinner substrate design. The design methodology is presented here using the conventional ground plane. This helps in realizing similar E-shape variations in the given specific frequency band.

Thus, simpler novel designs of E-shape MSAs offering separate operating bands for the wideband and CP response are the new technical contribution in the proposed work. Although the work presented in this paper is exhaustive, it provides a complete study for the wideband and CP variations of E-shape MSAs on thicker and thinner substrates. This kind of detailed study for antennas offering both wideband and CP responses individually is not reported in the available papers. Further, amongst all the configurations proposed in this paper, offset E-shape MSA using bow-tie shape ground plane offers optimum results in terms of impedance and AR BW, reduction in substrate thickness, and the broadside gain. Also the modified ground plane design is simpler in implementation against the beveled feed design.

6. CONCLUSIONS

Variations of E-shape MSAs are proposed for the wideband and CP response. Unlike the reported E-shape or U-slot cut variations for the CP response, in the proposed designs, two separate regions for the wideband and CP characteristics are achieved. The two antennas offer the total impedance BW of greater than 32% with AR BW of 4–5%, which lies towards the higher frequency region of the impedance BW. The designs using bow-tie shape ground plane are presented to reduce the electrical substrate thickness. In this, design of offset E-shape MSA offers 12% increases in the BW with $0.03\lambda_g$ reduction in the total substrate thickness. A beveled feed design of half E-shape MSA for the wideband and CP characteristics is presented, which yields similar response but with feed probe length of $0.022\lambda_g$. The resonant length formulation and subsequent design methodology are presented that help in designing similar antennas around the given frequency range as per the targeted application.

REFERENCES

1. Kumar, G. and K. P. Ray, *Broadband Microstrip Antennas*, Artech House, 2003.
2. Yoo, J. and H. W. Son, "A simple compact wideband microstrip antenna consisting of three staggered patches," *IEEE Antennas and Wireless Propagation Letters*, Vol. 19, No. 12, 2038–2042, 2020.
3. Wong, K. L., *Compact and Broadband Microstrip Antennas*, 1st Edition, John Wiley & Sons, Inc., New York, USA, 2002.
4. Huynh, T. and K. F. Lee, "Single-layer single-patch wideband microstrip antenna," *Electronic Letters*, Vol. 31, No. 16, 1310–1312, 1995.
5. Wong, K. L. and W. H. Hsu, "A broadband rectangular patch antenna with pair of wide slits," *IEEE Transactions on Antennas & Propagation*, Vol. 49, No. 9, 1345–1347, 2001.
6. Bhardwaj, S. and Y. R. Samii, "A comparative Study of C-shaped, E-shaped, and U-slotted Patch Antennas," *Microwave and Optical Technology Letters*, Vol. 54, No. 7. 1746–1756, 2012.
7. Ge, Y., K. P. Esselle, and T. S. Bird, "A compact E-shaped patch antenna with corrugated wings," *IEEE Transactions on Antennas & Propagation*, Vol. 54, No. 8, 2411–2413, 2006.
8. Babu, K. J., K. S. R. Krishna, and L. P. Reddy, "A modified E-shape patch antenna for MIMO systems," *International Journal of Computer science Engineering*, Vol. 2, No. 7, 2427–2430, 2010.
9. Deshmukh, A. A., D. Singh, and K. P. Ray, "Modified designs of broadband E-shape microstrip antennas," *Sadhana-Academy Proceedings in Engineering Science*, Vol. 3, No. 3, 44–64, 2019.
10. Radavaram, S. and M. Pour, "Wideband radiation reconfigurable microstrip patch antenna loaded with two inverted U-slots," *IEEE Transactions on Antennas & Propagation*, Vol. 67, No. 3, 1501–1508, 2018.
11. Deshmukh, A. A. and A. P. C. Venkata, "Wideband pentagonal shape microstrip antenna using a pair of rectangular slots," *Progress In Electromagnetics Research C*, Vol. 107, 113–126, 2021.
12. Liu, N. W., L. Zhu, and W. W. Choi, "A low-profile wideband aperture-fed microstrip antenna with improved radiation patterns," *IEEE Transactions on Antennas & Propagation*, Vol. 67, No. 1, 562–567, 2019.
13. Liu, N. W., L. Zhu, and W. W. Choi, "A differential-fed microstrip patch antenna with bandwidth enhancement under operation of TM_{10} and TM_{30} modes," *IEEE Transactions on Antennas & Propagation*, Vol. 65, No. 4, 1607–1614, 2017.
14. Sharma, S. K. and L. Shafai, "Performance of a novel ψ-shaped microstrip patch antenna with wide bandwidth," *IEEE Antennas Wireless Propagation Letters*, Vol. 8, 468–471, 2009.
15. Deshmukh, A. A. and G. Kumar, "Compact broadband E-shaped microstrip antennas," *Electronics Letters*, Vol. 41, No. 18, 989–990, 2005.
16. Khan, M. and D. Chatterjee, "Characteristic mode analysis of a class of empirical design techniques for probe-fed U-slot microstrip patch antennas," *IEEE Transactions on Antennas & Propagation*, Vol. 64, No. 7, 2758–2770, 2016.
17. Lu, J. H., H. C. Yu, and K. L. Wong, "Compact circular polarization design for equilateral-triangular microstrip antenna with spur lines," *Electronic Letters*, Vol. 34, No. 21, 1989–1990, 1998.
18. Lu, J. H., H. C. Yu, and K. L. Wong, "Single-feed circularly polarized equilateral-triangular microstrip antenna with a tuning stub," *IEEE Transactions on Antennas & Propagation*, Vol. 48, No. 12, 1869–1872, 2000.
19. Cao, W., B. Zhang, T. Yu, and H. Li, "A single-feed broadband circular polarized rectangular microstrip antenna with chip-resistor loading," *IEEE Antennas and Wireless Propagation Letters*, Vol. 9, 1065–1068, 2010.
20. He, S. and J. Deng, "Compact and single-feed circularly polarisedmicrostrip antenna with wide beamwidth and axial-ratio beamwidth," *Electronics Letters*, Vol. 53, No. 15, 1013–1015, 2017.
21. Zhang, X. and L. Zhu, "High-gain circularly polarized microstrip patch antenna with loading of shorting pins," *IEEE Transactions on Antennas & Propagation*, Vol. 64, No. 6, 2172–2178, 2016.

22. Zhang, X., L. Zhu, and N. Liu, "Pin-loaded circularly-polarized patch antennas with wide 3-dB axial ratio bandwidth," *IEEE Transactions on Antennas & Propagation*, Vol. 65, No. 2, 521–528, 2017.
23. Ding, K., C. Gao, D. Qu, and Q. Yin, "Compact broadband circularly polarized antenna with parasitic patches," *IEEE Transactions on Antennas & Propagation*, Vol. 65, No. 9, 4854–4857, 2017.
24. Wang, L. and Y. F. En, "A wideband circularly polarized microstrip antenna with multiple modes," *IEEE Open Journal of Antennas and Propagation*, Vol. 1, 413–418, 2020.
25. Sim, C. Y. D., Y. W. Hsu, C. W. Lin, and G. Yang, "Broadband circularly polarized antenna with moon-shaped parasitic element," *International Journal of RF and Microwave Computer-Aided Engineering*, Vol. 26, No. 5, 387–395, 2016.
26. Wei, K. and B. C. Zhu, "The novel W parasitic strip for the circularly polarized microstrip antennas design and the mutual coupling reduction between them," *IEEE Transactions on Antennas & Propagation*, Vol. 67, No. 2, 804–813, 2018.
27. Yang, W. W., W. J. Sun, W. Qin, J. X. Chen, and J. Y. Zhou, "Broadband circularly polarised stacked patch antenna with integrated dual-feeding network," *IET Microwaves, Antennas & Propagation*, Vol. 11, No. 12, 1791–1795, 2017.
28. Gautam, A. K., A. Kunwar, and B. K. Kanaujia, "Circularly polarized arrowhead-shape slotted microstrip antenna," *IEEE Antennas and Wireless Propagation Letters*, Vol. 13, 471–474, 2014.
29. Bernard, L. B. and A. Alphones, "An eshaped slotted circular patch antenna for circularly polarized radiation and radiofrequency energy harvesting," *Microwave and Optical Technology Letters*, Vol. 58, No. 4, 868–875, 2016.
30. Wei, K., J. Y. Li, L. Wang, R. Xu, and Z. J. Xing, "A new technique to design circularly polarized microstrip antenna by fractal defected ground structure," *IEEE Transactions on Antennas & Propagation*, Vol. 65, No. 7, 3721–3725, 2017.
31. Khidre, A., K. F. Lee, F. Yang, and A. Elsherbeni, "Wideband circularly polarized E-shaped patch antenna for wireless applications," *IEEE Antennas and Propagation Magazine* Vol. 52, No. 5, 219–29, 2010.
32. Lam, K. Y., K. M. Luk, K. F. Lee, H. Wong, and K. B. Ng, "Small circularly polarized U-slot wideband patch antenna," *IEEE Antennas and Wireless Propagation Letters*, Vol. 10, 87–90, 2011.
33. Tong, K. F. and T. P. Wong, "Circularly polarized U-slot antenna," *IEEE Transactions on Antennas & Propagation*, Vol. 55, No. 8, 2382–2385, 2007.
34. Deshmukh, A. A. and A. Odhekar, "Dual band circularly polarized modified ψ-shape microstrip antenna," *Progress In Electromagnetics Research C*, Vol. 115, 161–174, 2021.
35. Kovitz, J. M., H. Rajagopalan, and Y. Rahmat-Samii, "Circularly polarised half E-shaped patch antenna: a compact and fabrication-friendly design," *IET Microwaves, Antennas & Propagation*, Vol. 10, No. 9, 932–938, 2016.
36. Liu, S., W. Wu, and D. G. Fang, "Single-feed dual-layer dual-band E-shaped and U-slot patch antenna for wireless communication application," *IEEE Antennas and Wireless Propagation Letters*, Vol. 15, 468–471, 2015.
37. Chen, Y. and C. F. Wang, "Characteristic-mode-based improvement of circularly polarized U-slot and E-shaped patch antennas," *IEEE Antennas and Wireless Propagation Letters*, Vol. 11, 1474–1477, 2012.
38. Venkata, A., P. Chavali, and A. A. Deshmukh, "Wideband designs of regular shape microstrip antennas using modified ground plane," *Progress In Electromagnetics Research C*, Vol. 117, 203–219, 2021.